Supporting Information for

Valley manipulation by slidingly tuning the magnetic proximity effect in Heterostructures

Xikui Ma[a], Yingcai Fan[b], Weifeng Li[b], Yangyang Li[b], Xiangdong Liu[b], Xian Zhao[a,*], Mingwen Zhao[b,*]

[a] *Center for Optics Research and Engineering of Shandong University, Shandong University, Qingdao, 266237, China*

[b] *School of Physics, Shandong University, Jinan, Shandong, 250100, China*

* Corresponding authors: Email: xianzhao@sdu.edu.cn (XZ); zmw@sdu.edu.cn (MZ)

Section I

The detail of the $k \cdot p$ model of TMDs/AFM-I/TMDs.

The basic functions of TMDs were chosen as $|\Psi_{CB}^{\tau}>=|d_{z^2}>$ and $|\Psi_{VB}^{\tau}>=(|d_{x^2-y^2}+i\tau|d_{xy}>)/\sqrt{2}$, due to the main contribution of CBM and VBM are from d_{z^2} and $d_{x^2-y^2}/d_{xy}$. The Hamiltonian of upper TMDs monolayer (H_0^{up}) with consider SOC effect can be written as[1, 2]

$$H_0^{up}=\begin{pmatrix}\frac{\Delta}{2}+\varepsilon+\tau s\lambda_c & t_{12}(\tau q_x+iq_y)\\ t_{12}(\tau q_x-iq_y) & -\frac{\Delta}{2}+\varepsilon+\tau s\lambda_v\end{pmatrix}$$

in which Δ is band gap at K and K' valley, ε is on-site energy. The parameter $\tau=\pm 1$ is the adjacent corner of Brillouin zone. The $\vec{q}=\vec{k}-\vec{K}$ represents the momentum vector of electrons relative to the K (or K') point. t_{12} is the intralayer nearest-neighbor hopping integral. $s=\pm 1$ is the spin index which represents spin up and spin down. $\lambda_{c(v)}$ represents the spin splitting origin from SOC effect at CBM and VBM in monolayer.

Due to the 2H stacked TMDs bilayer, the Hamiltonian of lower TMDs monolayer (H_0^{lw}) can be written as

$$H_0^{lw}=\begin{pmatrix}\frac{\Delta}{2}+\varepsilon-\tau s\lambda_c & t_{12}(\tau q_x-iq_y)\\ t_{12}(\tau q_x+iq_y) & -\frac{\Delta}{2}+\varepsilon-\tau s\lambda_v\end{pmatrix}$$

When a magnetization was introduced into the upper TMDs monolayer, the exchange interaction (H_{ex}):

$$H_{ex}=\begin{pmatrix}-sm_c & 0\\ 0 & -sm_v\end{pmatrix}$$

Where $m_{c(v)}$ describes the exchange interaction in the conduction band (CB) and valence band (VB) in monolayer. The exchange interaction of lower TMDs monolayer is opposite to upper layer due to the opposite magnetization.

The polarized stacking leads to an electric field term H_E which induces an energy shift of $+U/2$ in one layer and $-U/2$ in another one layer:

$$H_E=I_2\otimes\frac{U}{2}$$

I_2 is the 2×2 identity matrix.

The distance between two TMDs monolayers is very large, rendering the interlayer hopping between VB and CB negligibly small. Here, we only consider the interlayer hopping for electrons to electrons (t_{cc}) and holes to holes (t_{vv}) , respectively, which are independent on the wavenumber. The interlayer hopping can be written as:

$$H_{\perp} = \begin{pmatrix} t_{cc} & 0 \\ 0 & t_{vv} \end{pmatrix}$$

We introduce a layer index (l) to describe the layer-resolved physical properties, the monolayer TMDs:

$$H^{up(lw)} = (H_0^{up(lw)} + l[H_{ex} + H_E])$$

Finally, the total Hamiltonian of TMDs/AFM-I/TMDs can be written as:

$$H_k = \begin{pmatrix} H^{up} & H_{\perp} \\ H_{\perp} & H^{lw} \end{pmatrix}$$

Section II

1. The lattice properties of MnO monolayer

The MnO monolayer adopt the trigonal symmetry with P-3m1 space group，which is composed of two bucked honeycomb MnO sublayers with rotating 180° from each other, as shown in Fig. S1 (a). The primitive cell of MnO monolayer contains two Mn atoms and two O atoms, and the buckling height is 0.19 Å. The smaller buckling height of MnO monolayer compare to MnX (X=S, Se, Te) monolayer lead to more exposed Mn atoms which beneficial for magnetic proximity effect. The optimized lattice constant of MnO monolayer is 3.55 Å. In addition, we verified the dynamic stability of the MnO monolayer by calculating the phonon spectrum. It is found that the phonon spectrum is free from imagery frequency modes, as shown in Fig. S1(b), suggesting that it is stable once synthesized.

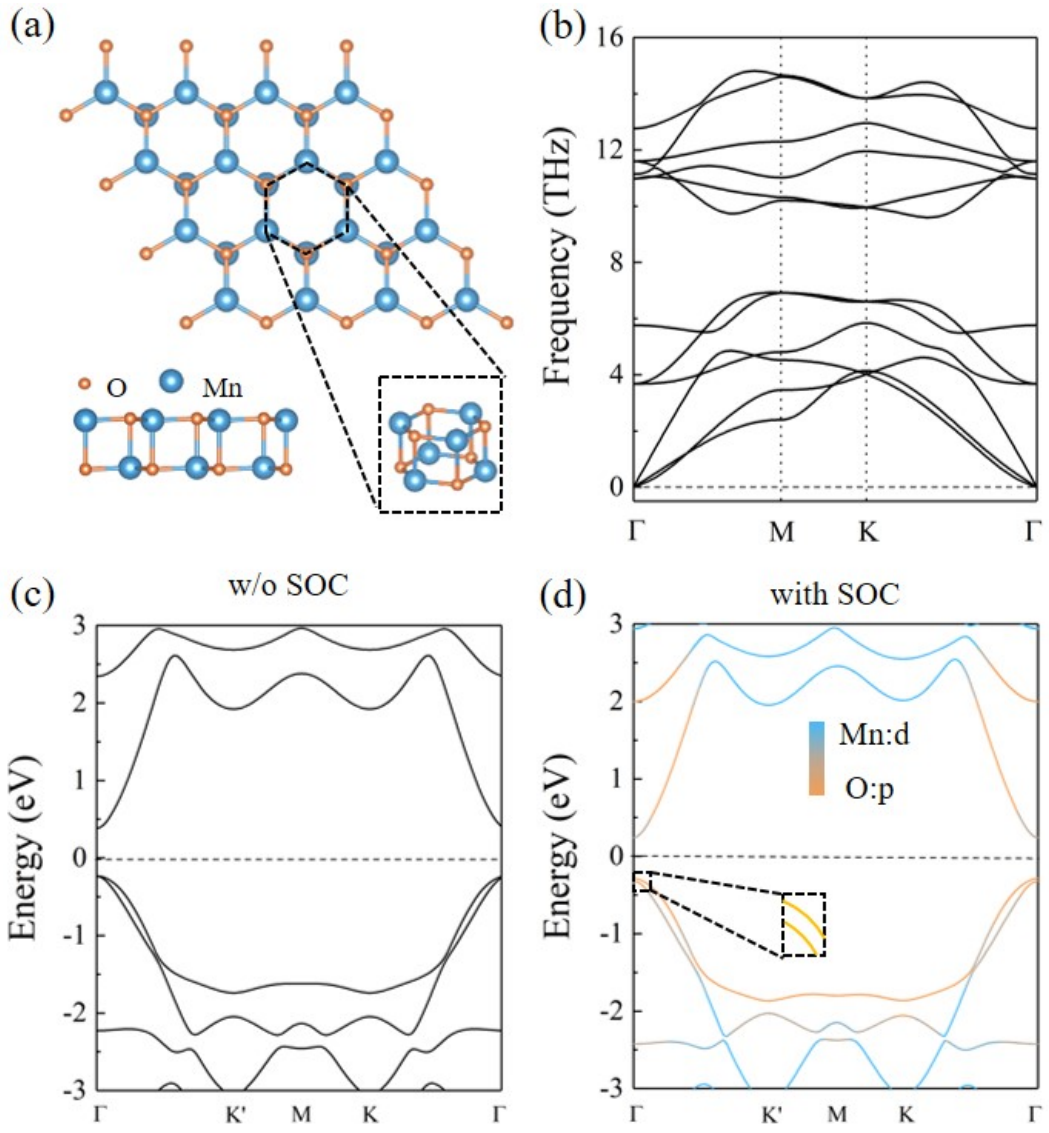

Fig. S1 (a) Top and side view of MnO monolayer. The orange and blue balls represent O and Mn atoms, respectively. (b) Phonon spectrum of MnO monolayer. (c-d) Band structure of MnO monolayer without/with SOC effect.

2. The electronic and antiferromagnetic properties of MnO monolayer

The electronic band structure of MnO monolayer without SOC effect is depicted in Fig. S1(c). We can see the VBM and CBM are both present at the Γ point with a direct band gap of 0.61 eV. In the presence of the SOC effect, the energy degeneracy at the Γ point is lifted as shown in Fig. S1(d), which shows a direct band gap of 0.52 eV. However, the band structure is spin degenerate due to the AFM order. The analysis of orbital indicates the VBM and CBM are predominantly of *p* character of the O atoms,

whereas the contribution of Mn-d orbital is little away from the Fermi level.

We next discuss the magnetic properties of MnO monolayer. Our calculations indicate the Neel-type AFM is the most stable magnetic configuration, which is more stable than the FM states by about 0.16eV per unit cell. The AFM states and two-type Mn atoms (top and bottom sublayers) guarantee the opposite spin equally distribute into two sides. The magnetic anisotropy energy (MAE) calculations indicate that MnO monolayer favors out-of-plane magnetization rather than in-plane magnetization by about 0.1 meV, which is different from the MnX. In the ground state, each Mn atom in MnO monolayer has a magnetic moment of ~4.4 μB but pointing in opposite directions along out-of-plane.

Section III

The electric polarization of $MoTe_2$/MnO/$MoTe_2$ heterostructure

In conventional three-dimensional (3D) metallic materials, screen effect of itinerant electrons can counteract the electric polarization. However, for two-dimensional metallic materials, such as 2D ferroelectric materials, the screening effect along the out-of-plane direction is weaker compared to that in 3D materials, which renders them viable candidates. Experimental evidences for ferroelectric 2D metals, like two-or three-layer WTe_2, has been reported [Fei et al., Nature 560, 7718 (2018)].

In the context of the $MoTe_2$/MnO/$MoTe_2$ heterostructures considered in this work, the electronic band structures at the equilibrium state (no strain) exhibit p-type semiconducting feature, as depicted in Fig. S2. The limited screening effect of the carriers (holes) fails to eliminate the potential electric polarization. This can be evidenced by the electrostatic potential difference (EPD) between the two sides of the heterostructures at the vacuum levels. However, the Berry phase method is not directly applicable for accessing the electric polarization of the p-type-semiconducting $MoTe_2$/MnO/$MoTe_2$ heterostructures. Fortunately, by inducing compressive strain, the Fermi level of the heterostructures can be adjusted into the band gap, as shown in Fig. S3, enabling the application of the Berry phase method work. With a stain value of $\triangle$d=-5%, our calculations yielded an electric polarization of ~32×10^{-12} C/m using the Berry phase approach. It is interesting to find that the difference in EPD between the strained and unstrained $MoTe_2$/MnO/$MoTe_2$ heterostructures is approximately lower than 0.01 eV. From this, we infer that the $MoTe_2$/MnO/$MoTe_2$ heterostructures have an electric polarization (~10^{-12} C/m) along the out-of-plane direction.

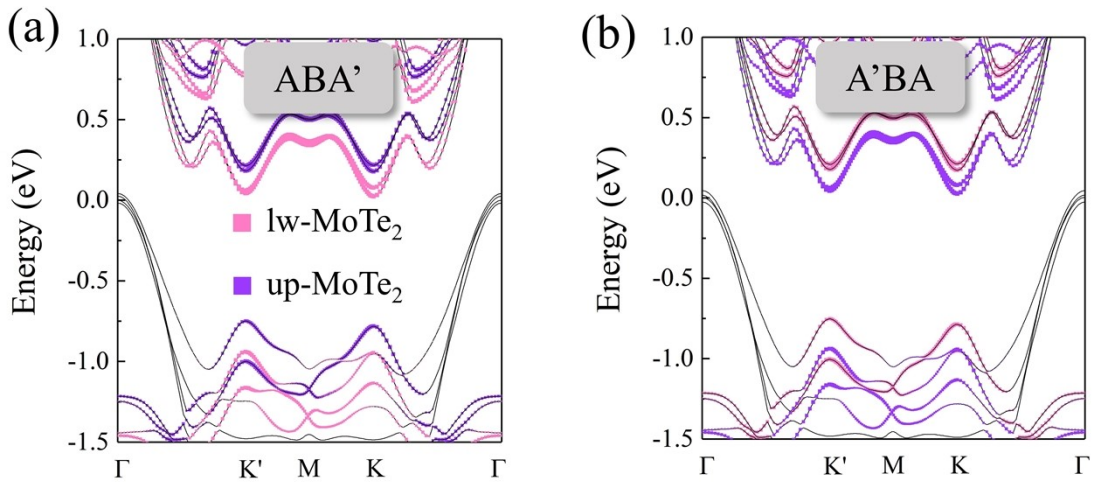

Fig. S2 (a-b) The contribution of lower and upper $MoTe_2$ monolayer in band structures. The black line represents the MnO monolayer.

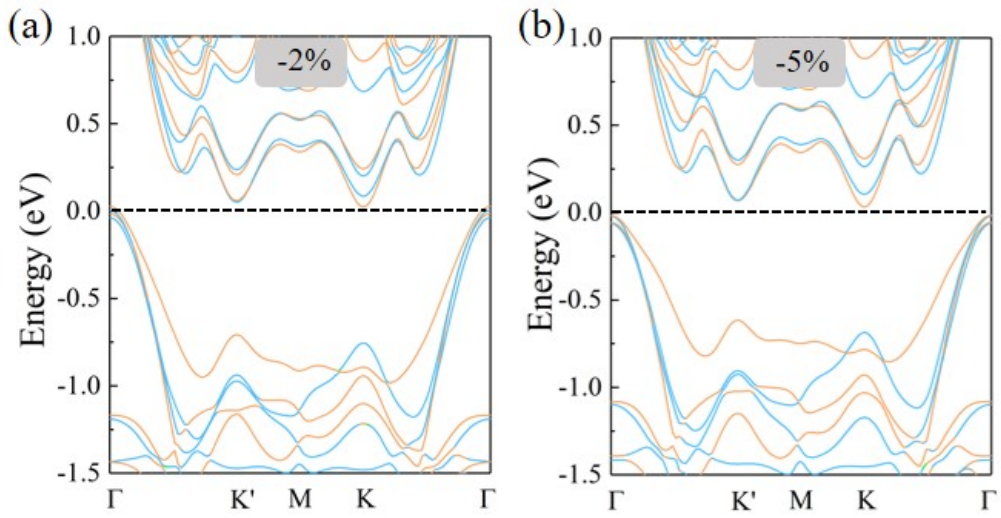

Fig. S3 (a-b) Band structures of ABA' and A'BA states with SOC when interlayer distance decreases (△d=-2%, -5%).

Section IV

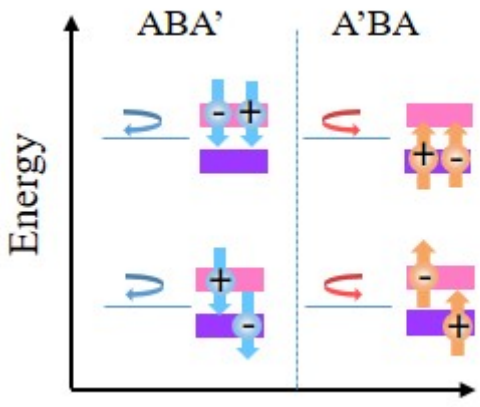

Fig. S4 Valley optical selective rules for intra/interlayer triplet exciton emission near K' valley in ABA' and A'BA state.

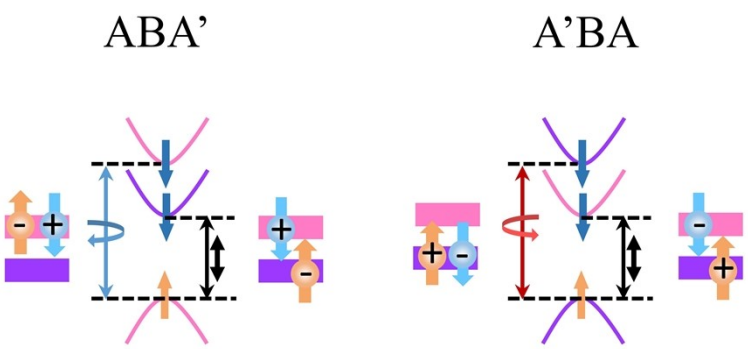

Fig. S5 Valley optical selective rules for intra/interlayer singlet exciton emission near K' valley in ABA' and A'BA state. The orange and blue arrow represent the spin. The pink and purple line represent the contributions of upper and lower $MoTe_2$ monolayers. The blue and red curved arrows represent the selective absorption of the left and right polarized light in interband transition, respectively. The thick vertical arrows represent the selective absorption disappear.

Reference

1. D. Xiao, G. B. Liu, W. Feng, X. Xu, and W. Yao, *Phys. Rev. Lett.,* 2012, **108**, 196802.

2. A. Kormányos, G. Burkard, M. Gmitra, J. Fabian, V. Zólyomi, N. D. Drummond, and V. Fal'ko, *2D Mater.,* 2015, **2**, 022001